NMR Structure of the Second Intracellular Loop of the α2A Adrenergic Receptor: Evidence for a Novel Cytoplasmic Helix[†,‡]

Duane A. Chung,[§,||] Erik R. P. Zuiderweg,[*,§,⊥,#] Carol B. Fowler,[▽] Orkun S. Soyer,[#] Henry I. Mosberg,[§,▽] and Richard R. Neubig[*,§,||,▼]

Biophysics Research Division and Departments of Pharmacology, Biological Chemistry, Chemistry, Medicinal Chemistry, and Internal Medicine/Hypertension, The University of Michigan, Ann Arbor, Michigan 48109

Received September 27, 2001; Revised Manuscript Received December 11, 2001

ABSTRACT: A major, unresolved question in signal transduction by G protein coupled receptors (GPCRs) is to understand how, at atomic resolution, a GPCR activates a G protein. A step toward answering this question was made with the determination of the high-resolution structure of rhodopsin; we now know the intramolecular interactions that characterize the resting conformation of a GPCR. To what degree does this structure represent a structural paradigm for other GPCRs, especially at the cytoplasmic surface where GPCR−G protein interaction occurs and where the sequence homology is low among GPCRs? To address this question, we performed NMR studies on ∼35-residue-long peptides including the critical second intracellular loop (i2) of the α2A adrenergic receptor (AR) and of rhodopsin. To stabilize the secondary structure of the peptide termini, 4−12 residues from the adjacent transmembrane helices were included and structures determined in dodecylphosphocholine micelles. We also characterized the effects on an α2A AR peptide of a D130I mutation in the conserved DRY motif. Our results show that in contrast to the L-shaped loop in the i2 of rhodopsin, the i2 of the α2A AR is predominantly helical, supporting the hypothesis that there is structural diversity within GPCR intracellular loops. The D130I mutation subtly modulates the helical structure. The spacing of nonpolar residues in i2 with helical periodicity is a predictor of helical versus loop structure. These data should lead to more accurate models of the intracellular surface of GPCRs and of receptor-mediated G protein activation.

G protein coupled receptors (GPCRs)[1] comprise a large and diverse family of receptors, each of which contains seven transmembrane (TM) spanning helices and activates an associated heterotrimeric G protein. Recently, Palczewski et al. solved the first high-resolution structure of a prototypical GPCR, rhodopsin (*1*), which activates the G protein transducin. This structure provided an important piece to the puzzle of GPCR-mediated signal transduction. While this accomplishment represents a large step forward on the path toward a complete understanding of GPCR mechanisms, this lone structure of an inactive-state GPCR leaves unanswered the question of how rhodopsin and other GPCRs actually activate their G proteins. The laboratory of Khorana (*2*, *3*) and others (*4*) have recently provided information on the conformational changes that occur during activation and the molecular interactions that form between rhodopsin and transducin.

Rhodopsin has been the focus of GPCR biophysical studies because of the ability to obtain working quantities of the purified, stable, nonaggregated receptor. However, the applicability of the rhodopsin paradigm to other GPCRs is a matter of speculation (*5*). The seven TM helices contain several residues that are highly conserved among rhodopsin-like GPCRs (*6*), and, thus, the seven-TM bundle of rhodopsin likely provides a good three-dimensional template for other GPCRs (*7*). However, in the intracellular loops, there are very few conserved residues (*6*). Together with the considerable variability in length of the third intracellular loop (*8*), this suggests that the intracellular surface of GPCRs, which forms the GPCR−G protein interface, may be structurally dissimilar. Despite this possibility, investigators often utilize rhodopsin structural data to model the intracellular surface

[†] This work was supported by NIH Grants HL46417 and GM59462 (R.R.N.), NIH Grant DA03910 (H.I.M.), and by a National Sciences and Engineering Research Council of Canada Postgraduate Scholarship (APP 207830-1998) (D.A.C.). E.R.P.Z. was partially supported by NIH Grant GM52421.

[‡] The atomic coordinates for T3-I2 and T3-I2(D130I) (code 1HLL) were deposited in the Protein DataBank, Research Collaboratory for Structural Bioinformatics, Rutgers University, New Brunswick, NJ (http://www.rcsb.org/). The chemical shifts were deposited in the BioMagResBank [accession codes 5143 (wild-type T3-I2), 5144 (Rho-T3-I2-T4), 5149 (mutant T3-I2(D130I)), and 5150 (T3-I2-T4)].

* To whom correspondence should be addressed. R.R.N.: Department of Pharmacology, The University of Michigan Medical School, 1301 MSRB III, 1150 W. Medical Center Dr., Ann Arbor, MI 48109-0632. Phone: (734) 763-3650. Fax: (734) 763-4450. E-mail: RNeubig@med.umich.edu. E.R.P.Z.: Biophysics Research Division, The University of Michigan, 930 N. University Ave., Ann Arbor, MI 48109. Phone: (734) 936-3850. Fax: (734) 764-3323. E-mail: zuiderwe@umich.edu.

[§] Biophysics Research Division.

[||] Department of Pharmacology.

[⊥] Department of Biological Chemistry.

[#] Department of Chemistry.

[▽] Department of Medicinal Chemistry.

[▼] Department of Internal Medicine/Hypertension.

[1] Abbreviations: GPCR, G protein coupled receptor; TM, transmembrane; i2, second intracellular loop; DRY motif, conserved Glu/Asp-Arg-Tyr tripeptide at the N-terminus of i2; T3-I2(D130I), T3-I2 peptide with a D130I mutation; AR, adrenergic receptor; DPC, dodecylphosphocholine; WT, wild-type; NOE, nuclear Overhauser effect; NOESY, NOE spectroscopy; $^3J_{HN\alpha}$, vicinal spin−spin coupling constants between the backbone amide proton and the α-proton; COSY, correlation spectroscopy; TOCSY, total correlation spectroscopy; RMSD, root-mean-square deviation; mAchR, muscarinic acetylcholine receptor; G_o/G_i, inhibitory G protein.

10.1021/bi015811+ CCC: $22.00
Published on Web 02/21/2002

of other GPCRs, and then utilize these models to analyze the activation mechanisms of GPCRs and GPCR−G protein interactions (*9*−*11*). This would seem to be a reasonable approach in the absence of actual structural data that confirm differences in GPCR structure and based on Baldwin's prediction that each of the TM helices would extend a similar length into the cytoplasm in rhodopsin-like GPCRs (*6*). However, in a recent mutagenesis study of the α2A adrenergic receptor (AR), we observed functional and structural differences with rhodopsin that challenged the appropriateness of the rhodopsin structural paradigm to the intracellular surface of the α2A AR (Chung et al., submitted for publication). We found that a D130I mutation in the conserved DRY motif in the second intracellular loop (i2) did not induce constitutive activity as seen for mutations at the homologous residue in several other GPCRs (*12*, *13*), including rhodopsin (*14*). In the same study, circular dichroism spectroscopy of peptides derived from the α2A AR i2 suggested that they contained considerably more helical structure than rhodopsin's i2. Developing an accurate structural model of the i2 loop is important since this loop is a critical part of the G protein-binding surface and it is believed to be a switch controlling receptor activation (*15*). Mutations in i2 disrupt receptor−G protein coupling (*15*−*17*), and peptides from i2 competitively inhibit receptor−G protein interactions (*18*−*20*).

In this report, we solve the NMR structures of wild-type α2A AR i2 peptides and a D130I mutant peptide in a membrane-like environment, dodecylphosphocholine (DPC) micelles, and compare them to structural features of a similar peptide from rhodopsin. The peptides contain up to 12 residues from the adjacent TM3 and TM4 helices flanking the i2 loop. We were able to identify the location of helical structure within these peptides. We also evaluated the limits of these peptides as structural models of the intact receptor by comparing the NMR-derived secondary structure of an i2 peptide from rhodopsin to that in the crystal structure. Our results demonstrated the presence of a novel cytoplasmic helix in the α2A AR i2, which is absent in the i2 of rhodopsin and in the rhodopsin i2 peptide. This provides new experimental data showing that while the TM bundles in GPCRs may be similar, the intracellular surface of GPCRs is structurally diverse.

EXPERIMENTAL PROCEDURES

Peptide Synthesis. The T3-I2-T4 peptide (Figure 1) and the Rho-T3-I2-T4 peptide (Figure 10) were synthesized on an ABI 431A synthesizer using standard *N*-(9-fluorenyl)-methoxycarbonyl protection methods. Double piperidine deprotection cycles, double coupling with 2-(1*H*-benzotriazol-1-yl)-1,1,3,3-tetramethyluronium hexafluorophosphate, and acetic anhydride capping after each double-coupled cycle were utilized to improve deprotection and coupling efficiency and to guard against the formation of deletion peptides. The Rho-T3-I2-T4 peptide was ^{15}N-labeled at the backbone NH resonance of Val-129 and Val-138 to facilitate resonance assignment. The 32-residue T3-I2 peptide and its D130I mutant analogue, T3-I2(D130I) (Figure 1), were synthesized and purified by Quality Controlled Biochemicals (Hopkinton, MA), with acetylated N-termini to facilitate micelle insertion. Likewise, the T3-I2-T4 and Rho-T3-I2-T4 peptides were acetylated at their N-termini and amidated at their C-termini.

Peptide purity and structure were confirmed by HPLC and mass spectrometry; they were greater than 90% pure. The sequences of T3-I2 and T3-I2-T4 correspond to residues 118−149 and 121−155, respectively, of the human α2A AR (*21*), and Rho-T3-I2-T4 corresponds to residues 125−158 of bovine type I rhodopsin.

NMR Sample Preparation. The lyophilized peptide was dissolved in water containing 657 mM dodecylphosphocholine-d_{38} (DPC) (Cambridge Isotope Laboratories, Andover, MA) and diluted with buffer to give final sample conditions of 0.9 mM peptide, 460 mM DPC, 10% D_2O/90% H_2O, 50 mM NaCl, 10 mM NaH_2PO_4, pH 4.5. Samples were also prepared in the same buffer conditions with 100% D_2O. Freshly prepared samples were used in each set of experiments to minimize line broadening in the spectra.

NMR Spectroscopy and NMR Structure Calculations. NMR spectra were acquired on a Varian INOVA 800 spectrometer equipped with a (^{1}H/^{13}C/^{15}N) triple resonance probe with pulsed field gradients. All NMR spectra were recorded at 303 K. Homonuclear two-dimensional TOCSY (31 and 86 ms mixing times) and NOESY spectra [with mixing times of 50 and 100 ms for T3-I2, 100 ms for T3-I2(D130I) and T3-I2-T4, and 50 ms for Rho-T3-I2-T4] were used to obtain the sequential assignments (*22*). We assigned side-chain resonances using TOCSY and NOESY spectra. A phase-sensitive COSY spectrum on T3-I2 helped to discriminate between H^β and H^γ protons, but lacked most of the resonances. JUMP−RETURN (*23*) and WATERGATE (*24*) pulse sequences before acquisition were used for water suppression in the TOCSY and NOESY experiments. For the COSY experiment, presaturation during the relaxation delay was used for water suppression. The spectral widths were typically 12 000 Hz in $\omega 2$ and 8000 Hz in $\omega 1$. Two hundred t_1 experiments with between 24 and 48 transients and 1184 complex t_2 points were recorded. The method of States-TPPI was used for quadrature detection in t_1 (*25*). Experimental parameters were identical for the wild-type T3-I2 and mutant T3-I2(D130I). The proton chemical shifts were referenced to the H_2O signal located at 4.764 ppm downfield from internal 4,4-dimethyl-4-silapentane-1-sulfonate (0.00 ppm), included in the Rho-T3-I2-T4 sample.

The NMR data were processed with NMRPipe software (*26*) and analyzed with a combination of NMRView (*27*), SPSCAN (*28*), and XEASY (*29*). TOCSY and NOESY data were zero-filled to 4K × 1K matrixes and apodized by a 30°-shifted sinebell window function prior to Fourier transformation. The COSY data were apodized by a sinebell in t_2 and a 48°-shifted sinebell in t_1. For all data sets, polynomials were subtracted from the time domain and the frequency domain data to achieve solvent subtraction and automatic baseline corrections, respectively. For T3-I2, all carbon-bound protons were assigned except for His-123 H^ϵ, Leu-124 H^δ, Ile-127 H^ϵ, Trp-133 $H^{\epsilon 1}$, Tyr-141 H^ϵ, Leu-143 H^δ, Lys-144 H^δ, H^ϵ, and Arg-149 H^δ. For T3-I2(D130I), the carbon-bound protons His-123 H^ϵ, Trp-133 $H^{\epsilon 1}$, Tyr-141 H^ϵ, and Arg-149 H^δ were not assigned. Of the exchangeable protons, only Arg-131 H^η was assigned. For T3-I2-T4 and Rho-T3-I2-T4, our goal was to determine their secondary structure and not to calculate their three-dimensional structure. Thus, for these two peptides, we assigned the H^N, H^α, and H^β protons, and only a small number of the remaining side-chain protons. The chemical shifts were deposited in

the BioMagResBank and are provided in the Supporting Information. For each of the ^{15}N-labeled valines in Rho-T3-I2-T4, the average of their split H^N resonances was deposited.

$^3J_{HN\alpha}$ coupling constants were estimated from the COSY spectrum (for those T3-I2 residues with observable cross-peaks) by measurements of separations of extrema in dispersive and absorptive plots of multiple rows through cross-peaks (*30*). For this spectrum, the digital resolution after zero-filling was 1.5 Hz/point.

NOE constraints for the structure calculations or secondary structure determination were extracted from the NOESY spectra [with mixing times of 50 ms for T3-I2 and Rho-T3-I2-T4 and 100 ms for T3-I2(D130I) and T3-I2-T4]. A small number of additional upper bounds were obtained from a T3-I2 NOESY spectrum at 100 ms mixing time and from NOESY spectra of T3-I2 and T3-I2(D130I) samples in 100% D_2O (100 ms mixing time). (These NOEs were assigned to upper distance limits of 5, 6, or 7 Å depending on their intensity.) Cross-peak volumes were corrected for the effects of JUMP−RETURN and converted to distances using the subroutine CALIBA (*31*) in DYANA (*32*). The distances were calibrated using a distance of 2.5 Å for the aromatic protons of Trp-133, and the distances were increased by 20% for use as upper bound constraints. For the α2A AR T3-I2, 426 ^{1}H-^{1}H NOEs and 11 coupling constants were obtained; for T3-I2(D130I), 452 ^{1}H-^{1}H NOEs were obtained. Using data processing with the DYANA subroutine FOUND (*33*), the data were converted into distance constraints [104 intraresidue, 92 short-range, 80 medium-range for T3-I2; 108 intraresidue, 93 short-range, and 79 medium-range for T3-I2(D130I); 172 total for T3-I2-T4 and 174 total for Rho-T3-I2-T4] and torsion angle constraints [144 for T3-I2 and 148 for T3-I2(D130I)]. No stereospecific assignments were made. Based on initial structures, one additional NOE was assigned using the subroutine ASNO (*34*). The final round of structure calculations with DYANA, for T3-I2 and T3-I2(D130I), started with 100 random structures, and the 20 conformers with the lowest residual target functions were chosen to represent the solution conformations of the peptides. No further energy minimization was performed on the conformers due to the unsuitability of standard force fields to describe environments containing micelles.

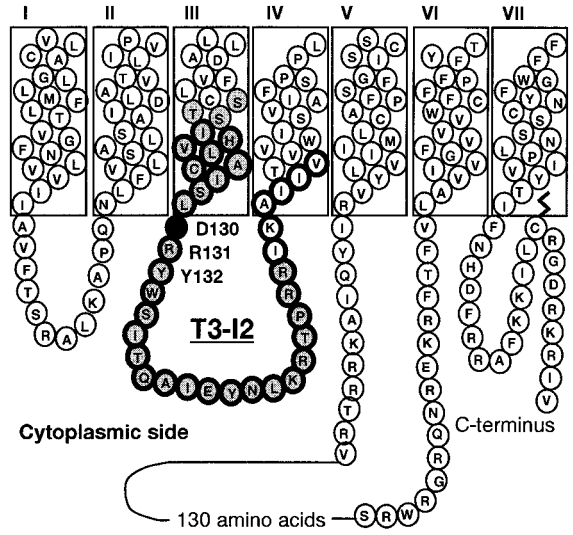

FIGURE 1: Topological model of the α2A AR showing the putative transmembrane and cytoplasmic domains based on Baldwin (*6*). The α2A AR T3-I2 peptide used in this study is shown as gray shaded circles. The T3-I2-T4 peptide is shown as black outlined circles. The location of Rho-T3-I2-T4 corresponds to the location of T3-I2-T4, with sequences aligned according to the location of the DRY motif. The residues of the DRY motif are labeled, and the black filled circle indicates the Asp-130 residue that was mutated.

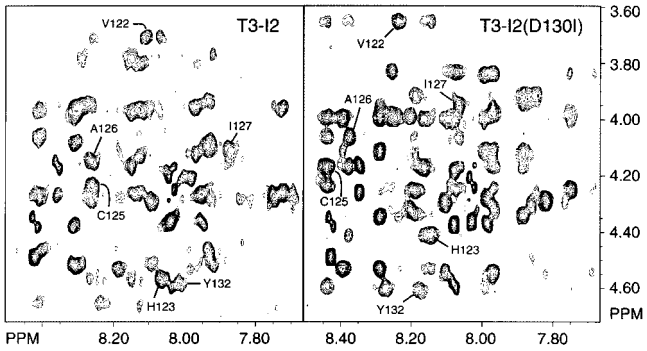

FIGURE 2: Portions of 800-MHz NOESY spectra of wild-type and mutant α2A AR T3-I2 peptides in DPC micelles. The mixing time was 50 ms for WT T3-I2 and 100 ms for mutant T3-I2(D130I). The experiments were performed in 460 mM DPC-d_{38}, pH 4.5, at 30 °C. Some of the sequential $d_{\alpha N}(i,i+1)$ connectivities that underwent changes in chemical shifts between the WT and the mutant T3-I2 peptide are labeled.

RESULTS

NMR Spectroscopy. Based on the GPCR model of Baldwin (*6*), the 32-residue T3-I2 peptide includes approximately 12 membrane-embedded residues from TM3 and almost the entire i2 loop (Figure 1). The T3-I2 peptide was insoluble in aqueous solutions but was soluble in dodecylphosphocholine (DPC) micelles. DPC micelles provide a zwitterionic lipid environment, and due to their small size (~19.7 kDa), they tumble rapidly and are amenable to solution NMR studies (*35*, *36*). Results for other membrane-associated peptides indicate only minor structural differences in DPC micelles and lipid bilayers (*37*). We performed the NMR experiments with freshly prepared samples, as sample aggregation was evident within 1 week of storage. Chemical shift assignments were nearly complete for the wild-type (WT) T3-I2 peptide and a mutant peptide, T3-I2(D130I), with a D130I mutation. High-quality NOESY spectra for the WT and mutant T3-I2 peptides were obtained and showed that several backbone NH−αH NOE cross-peaks changed in the spectrum of T3-I2(D130I), indicating mutation-induced conformational changes (Figure 2). After solving the structures of T3-I2 and T3-I2(D130I), we wanted to evaluate carefully the limitations of these peptides as structural models and, specifically, to determine whether the omission of TM4 residues might have generated artifacts. To do so, we used NMR to solve the secondary structure of a 35-residue T3-I2-T4 peptide, which contained 9 residues from TM3 and 4 residues from TM4, according to the Baldwin model (*6*) (Figure 1). We also studied a peptide, Rho-T3-I2-T4, of the corresponding domain from rhodopsin (see Figure 10 for the sequence of Rho-T3-I2-T4).

Secondary Structure of T3-I2 and T3-I2(*D130I*). The secondary shifts for the α protons, calculated by subtracting the experimentally measured chemical shifts from reference chemical shifts of an unstructured peptide and averaging over

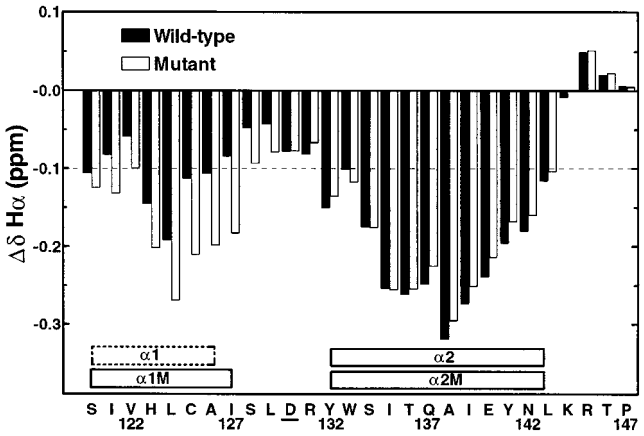

FIGURE 3: Secondary shifts of the α-protons of wild-type (solid bars) and mutant (open bars) T3-I2 peptide. The secondary shifts $\Delta\delta(^1H^\alpha)$ were calculated as the difference between the measured chemical shifts and the corresponding random coil chemical shifts, averaged over 5 residues (*38*). Rectangles indicate the location of helices derived from these data (see text). The mutated residue, D130, is underlined. The secondary shifts of the terminal 2 residues on each end of the peptide were not calculated since there would be fewer than 5 residues to average.

FIGURE 4: Summary of the sequential and medium-range NOEs for the T3-I2 peptides. Sequential NOEs $d_{\alpha N}$, d_{NN}, and $d_{\beta N}$ for the wild-type T3-I2 (A) and mutant T3-I2(D130I) (B) are presented as black bars with a thickness that corresponds to the intensity of the NOE. The medium-range connectivities $d_{\alpha N}(i,i+3)$ and $d_{\alpha\beta}(i,i+3)$ are shown by lines starting and ending at the positions of the residues related by the NOE. Rectangles correspond to helices identified in the secondary shift analysis, while dashed rectangles indicate additional helical structure revealed by the NOE patterns. Panel C shows the NOEs that were unambiguously present only in the WT (solid lines) or mutant (dashed lines) T3-I2 peptides. Numbers indicate the residue number in the α2A AR. In the row $^3J_{HN\alpha}$, filled circles indicate residues with $^3J_{HN\alpha} > 7$ Hz. The mutated residue, Asp-130, is underlined.

five residues, provide tentative information on the presence of secondary structure (*38*). Helical structure is indicated by a series of secondary shift values more negative than −0.1 ppm (*38*). According to this criterion, there is a potential helix spanning residues 120−126 (helix α1) in the WT T3-I2 peptide (Figure 3). (Residue numbering is based on the full-length α2A AR.) The secondary shifts of residues 127−131, including D130 and R131 of the DRY motif, while negative, are all more positive than −0.1 ppm, suggesting that helical structure, if present, may be flexible in this region. There is an indication of a second helix spanning residues 132−143 (helix α2). The strong negativity of the secondary shift values suggests that helix α2, which extends through most of the predicted i2 loop domain of the peptide, is very stable. The extreme carboxyl-terminal residues, Lys-144 to Arg-149, of the WT T3-I2 peptide are probably disordered.

In the D130I mutant peptide, there is an increase in the negativity of the secondary shifts over the N-terminal residues 120−128, suggesting that helix α1 is more stable and also 1−2 residues longer at its C-terminus in the mutant peptide, where it is referred to as helix α1M. The secondary shift values over residues 130−147 change very little in the mutant peptide, indicating that helix α2 is unchanged in the mutant peptide, where it is referred to as helix α2M.

NOE connectivities provide an independent measure of secondary structure. They are also essential to validate the secondary shift analysis, since we cannot rule out an effect of the micelles on the chemical shift values. A series of medium-range $d_{\alpha N}(i,i+3)$ and $d_{\alpha\beta}(i,i+3)$ NOEs, hallmarks of helical structure (*22*), spanned almost the entire length of the WT and mutant T3-I2 peptides from residues 118 to 145 (Figure 4A,B). This is consistent with the α1 and α2 helices identified by the secondary shift analysis. It also confirms that there is helical structure in residues 128−131 between helix α1 and helix α2, which we denote as helix α*. The series of small secondary shift deviations in this region raise the possibility, but do not prove, that helix α* is flexible. Medium-range $d_{\alpha N}(i,i+3)$ NOEs, typical of helical structure (*22*), were unambiguously absent at residues 126, 130, and 131, consistent with the hypothesis that helix α* may be flexible or may not be a classical α-helix.

The pattern of NOEs for the mutant T3-I2(D130I) peptide was similar to that of the WT peptide, again supporting the presence of helical structure, denoted helix α*M, between helix α1M and helix α2M (Figure 4B). Additional medium-range NOEs were present in helix α1M of the mutant peptide that were not present in the WT peptide (Figure 4C), supporting the indication from the secondary shift analysis that helix α1 is more stable in the mutant peptide. The changes in NOE patterns in helix α*M, and around the N-terminus of helix α2M, were more complex, with both the WT and mutant T3-I2 peptides containing NOEs that were not present in the other. This suggested that subtle conformational changes occurred in this region.

Large $d_{\alpha N}(i,i+1)$ NOEs were present at residues 144−149 at the C-terminus of both peptides. Together with the absence of medium-range NOEs in this region, this corroborates the secondary shift data indicating that the C-terminus is disordered in the WT and mutant peptides.

We observed large $^3J_{HN\alpha}$ coupling constant values for residues 118−121 and 143−149 at the termini of the WT T3-I2 peptide, consistent with extended or disordered conformations for these residues in a significant population of the peptides (Figure 4A). Ile-127, at the C-terminus of helix α1, also had a large $^3J_{HN\alpha}$ value (>7 Hz), providing independent evidence that this residue resides in a flexible or extended structure. The remaining residues did not

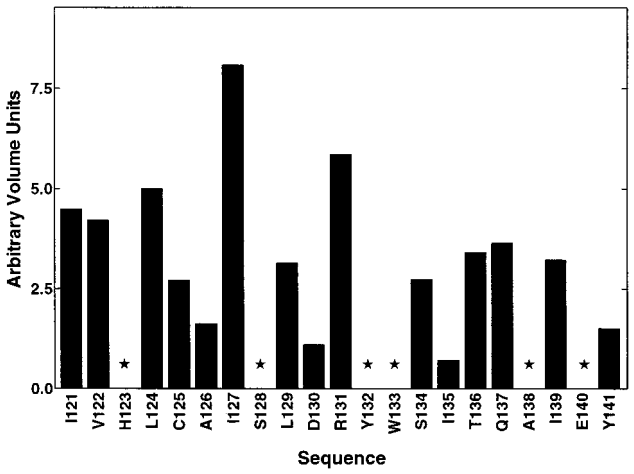

FIGURE 5: Volumes of HN−Hα cross-peaks in the helical regions of T3-I2, from TOCSY experiments with a mixing time of 31 ms. Data were obtained for the WT T3-I2 peptide in the presence of 460 mM DPC-d_{38}, pH 4.5, at 30 °C. Stars indicate residues for which volumes could not be determined due to resonance overlap.

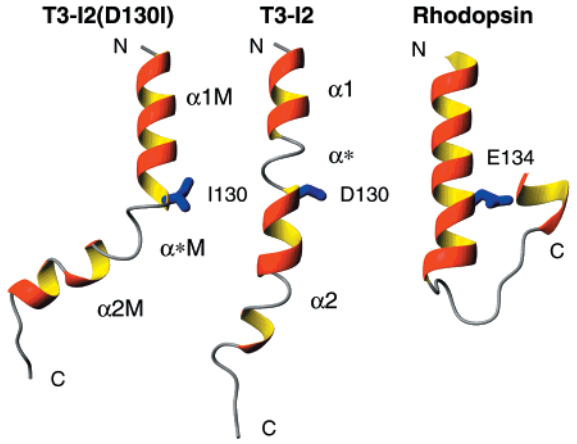

FIGURE 6: Comparison of the wild-type T3-I2, mutant T3-I2-(D130I), and rhodopsin structures. The backbones of the mean structures of wild-type T3-I2 and mutant T3-I2(D130I) peptides, and the corresponding region (residues 122−152) from the crystal structure of rhodopsin (*1*), are represented as ribbons. The mean peptide structures were calculated from a superposition of the 20 best DYANA conformers, for best fit of atoms N, C^{α}, and C′ of residues 120−142. Regular helices are colored red and yellow; more open helix-like regions, helix-like bends, and coil regions are colored gray. The helices are identified as α1, α*, and α2 in the wild-type T3-I2 and as α1M, α*M, and α2M in the mutant peptide. An interruption within helices α2 and α2M is likely due to NOEs that were missing as a result of spectral overlap. The chain ends are identified, and the side chains of the mutated residue, D130/I130, are colored blue. The rhodopsin structure is based on coordinates from the first molecule of Protein DataBank file 1F88. This figure and Figure 7 were prepared with the program MOLMOL (*48*).

generate cross-peaks of sufficient intensity or resolution from other cross-peaks in the COSY spectrum to extract coupling constants.

As an independent qualitative comparison of the $^3J_{HN\alpha}$ values within the helical regions of the WT T3-I2 peptide, we measured Hα−HN cross-peak volumes in the 31 ms mixing time TOCSY experiment (Figure 5). At mixing times <50 ms, this cross-peak volume is proportional to the magnitude of the $^3J_{HN\alpha}$ value (*39*). The Hα−HN cross-peak volume of Ile-127 was more than 1.5 times as large as that of any other residue in helix α1 or helix α2, except for Arg-131, supporting a larger $^3J_{HN\alpha}$ value that would be consistent with unstable helical structure in helix α* (Figure 5).

Altogether, the secondary shifts, the $^3J_{HN\alpha}$ coupling constants, and the NOEs describe a single helix spanning residues 118−143 in both the WT and mutant peptides. The helix appears to have three domains. Helix α1 (residues 118−126 in the WT T3-I2 and residues 118−127 in the mutant) in the transmembrane domain of the peptides and helix α2 (residues 132−143 in both peptides) in the cytoplasmic domain of the peptides are stable, α-helices. Helix α* (residues 127−131 in the WT and residues 128−131 in the mutant) separating helices α1 and α2 likely contains more flexible or irregular helical structure. In the mutant peptide, helix α1 is more stable than in the WT peptide, and it extends one or two residues further into the cytoplasm.

NMR Structure of T3-I2 and T3-I2(*D130I*). For the WT and mutant T3-I2 peptides, we were able to collect sufficient unambiguous NOE distance constraints to calculate high-quality three-dimensional structures with the computer program DYANA (*32*). The mean structure of the 20 best DYANA conformers is helix-like from residues 118−143 for both T3-I2 and T3-I2(D130I) (Figure 6). The conformers were superimposed for best fit of the backbone heavy atoms (N, C^{α}, C′) over the helical residues 120−142. Helical bends separate helix α1 and helix α2 in both the WT and mutant mean structures and are consistent with the flexibility attributed to helix α*. In T3-I2, the bend centers on Ile-127 and Ser-128, while in the mutant it occurs at Tyr-132 and Trp-133, closer to the C-terminus. This results in an extension of the C-terminus of helix α1 by one helical turn in the mutant peptide (Figure 6). In the mean T3-I2(D130I) structure, the pronounced bend between helix α1M and helix α2M is exaggerated by the absence of two potential medium-range NOEs that were missing as a result of spectral overlap. When we included these NOEs in a test structure calculation, the bend of the mutant structure was similar to that of the WT, but its location was still closer to the C-terminus in the mutant structure. In the individual top 20 conformers, there was considerable variation in the bend angle in each peptide (data not shown), suggesting that the bend angle is dynamic, and that helix α1 and helix α2 are generally not collinear. The C-terminus of both peptides (approximately residues 143−149) is unstructured.

Of significance, in contrast to the predominantly helical cytoplasmic domain of the T3-I2 peptides, the i2 loop in rhodopsin shows a short helical extension of TM3 followed by an L-shaped loop (*1*) (Figure 6).

The surface of T3-I2 has a line of hydrophobic residues that surrounds helix α1 (Figure 7A,B). Helix α2 is amphipathic with polar residues on one side and a nonpolar patch of residues on the other. The C-terminus of T3-I2 is highly positively charged.

Secondary Structure of T3-I2-T4 and Rho-T3-I2-T4. The novel cytoplasmic helix α2 that is absent in the i2 of rhodopsin was a crucial finding, and it was critical to ensure that it was not an artifact of the absence of TM4 residues that would anchor the peptide's C-terminus in the micelle. Thus, we performed NMR on a 35-residue peptide, T3-I2-T4, containing 4−9 TM residues at each end of the peptide in the same NMR conditions used for the shorter T3-I2

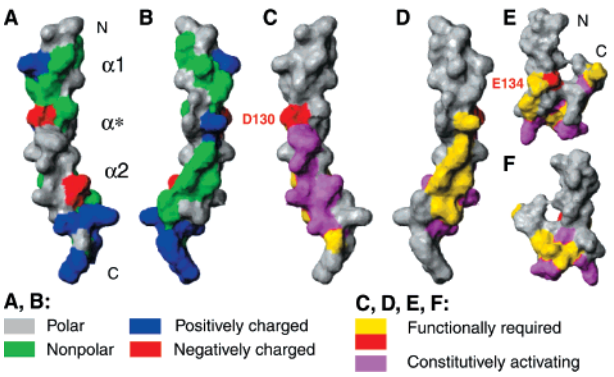

FIGURE 7: Surface representation of the mean structure of wild-type T3-I2 and rhodopsin. Panels A−D illustrate the α2A AR T3-I2 peptide structure, and panels E and F show the corresponding domain from rhodopsin (from the first molecule of Protein DataBank file 1F88). Panels A and B identify nonpolar (aliphatic; green), uncharged polar (hydroxyl, amine, sulfur-containing, and aromatics; gray), and charged residues (red and blue). The surfaces corresponding to helices α1, α*, and α2 are shown in panel A. Panels C through E show a mapping onto the surface of T3-I2 (C and D) and rhodopsin (E and F) of mutagenesis data from the m5 muscarinic receptor (*15*). Functionally required residues in the m5 muscarinic receptor i2 loop are red (Asp-130 and the homologous rhodopsin residue, Glu-134) and gold; constitutively activating mutant residues are magenta. Panels B, D, and F are generated from panels A, C, and E, respectively, by a 180° rotation about a vertical axis.

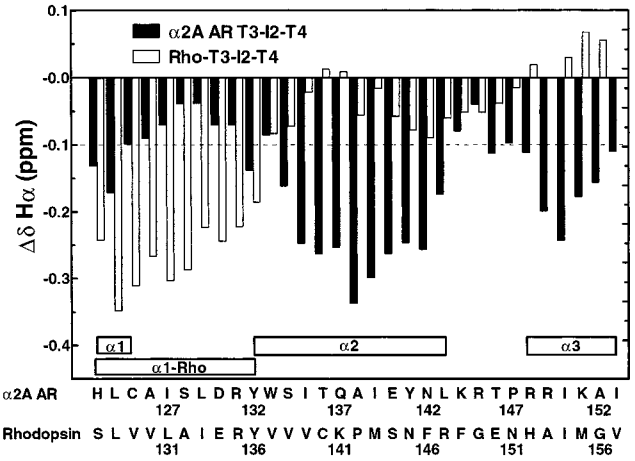

FIGURE 8: Secondary shifts of the α-protons of T3-I2-T4 (solid bars) and Rho-T3-I2-T4 (open bars). The T3-I2-T4 peptide contained transmembrane residues from both TM3 and TM4 flanking the intervening i2 loop (Figure 1), while the Rho-T3-I2-T4 peptide included the corresponding domain from rhodopsin. The secondary shifts $\Delta\delta(^1H^\alpha)$ were calculated as the difference between the measured chemical shifts and the corresponding random coil chemical shifts (*38*). Rectangles indicate the location of helices derived from these data.

peptides (see Figure 1 for the location of T3-I2-T4). The secondary shifts for the α protons indicate that T3-I2-T4 contains three helices (Figure 8). A probable helix α1 (residues 123−125) and a helix α2 (residues 132−143) are similar to the α1 and α2 helices in T3-I2. A third, new helix α3 formed in the TM4 residues (residues 148−153). The additional TM4 residues actually stabilized the C-terminus of helix α2 as shown by an average increase in the negativity of the secondary shift values compared to T3-I2, of 0.062 ppm per residue over residues 141−143. The pattern of unambiguous helical $d_{\alpha N}(i,i+3)$ and $d_{\alpha\beta}(i,i+3)$ NOEs measured for T3-I2-T4 corroborates the three helices suggested by the secondary shift distribution (Figure 9A). The cytoplasmic helix α2 contains a good density of overlapping $d_{\alpha\beta}(i,i+3)$ NOEs, indicating that it is the most stable of the three helices. Helical structure is again suggested for the residues between helix α1 and helix α2; however, the density of NOEs in this region and also in helix α1 is less compared to the NOE pattern of T3-I2, indicating that the helix in this region is now less stable. No medium-range NOEs cross through residues Ala-126-Ile-127 or Trp-133-Ser-134 in the T3-I2-T4 peptide, suggesting points of flexibility in the helices. Large $d_{\alpha N}(i,i+1)$ values, consistent with extended structures (*22*), were present at residues 127−129 and at the proline at residue 147, and provide evidence of helical breaks or distorted structure.

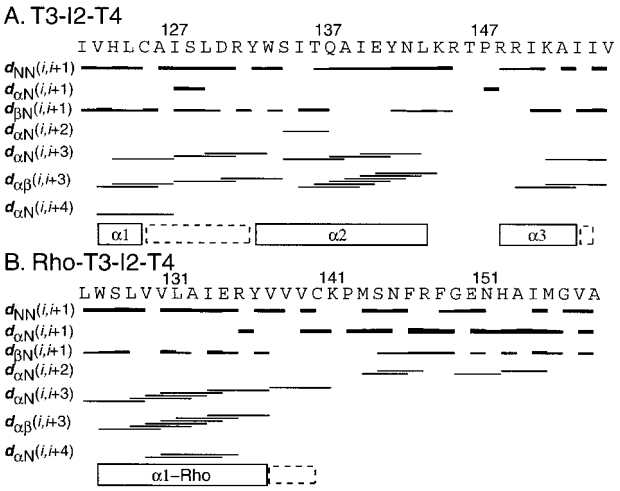

FIGURE 9: Summary of the sequential and medium-range NOEs for the T3-I2-T4 and Rho-T3-I2-T4 peptides. Sequential NOEs $d_{\alpha N}$, d_{NN}, and $d_{\beta N}$ for the T3-I2-T4 (A) and Rho-T3-I2-T4 (B) are presented as black bars with a thickness that corresponds to the intensity of the NOE. The medium-range connectivities $d_{\alpha N}(i,i+3)$ and $d_{\alpha\beta}(i,i+3)$ are shown by lines starting and ending at the positions of the residues related by the NOE. Rectangles correspond to helices that were indicated by the secondary shift analysis, while dashed rectangles indicate additional helical structure revealed by the NOEs.

To assess the validity of the peptide structures, we also performed NMR on a peptide derived from rhodopsin, Rho-T3-I2-T4, which we could compare to the rhodopsin crystal structure (*1*). The 34-residue Rho-T3-I2-T4 contains all of the residues homologous to T3-I2-T4 but is one residue shorter because rhodopsin's i2 is one residue shorter than that of the α2A AR. The secondary shifts for Rho-T3-I2-T4 indicate a single N-terminal helix, α1-Rho, that extends the TM3 helix into the i2 loop to rhodopsin residue 136 (Figure 8). No separate helix is present in the i2 loop, nor is any helix present in the TM4 residues. The pattern of sequential and medium-range $d_{\alpha N}(i,i+3)$ and $d_{\alpha\beta}(i,i+3)$ NOEs measured for Rho-T3-I2-T4 indicates that helix α1-Rho spans residues 125−137 and possibly extends to residue 140, and that there are no additional helices (Figure 9B). A pair of overlapping $d_{\alpha N}(i,i+2)$ NOEs spanning residues Met-143 to Phe-146 is consistent with the presence of a turn-like structure in the Rho-T3-I2-T4 peptide (*22*).

DISCUSSION

The GPCR field recently benefited from the high-resolution structure of rhodopsin (*1*). The challenge that remains

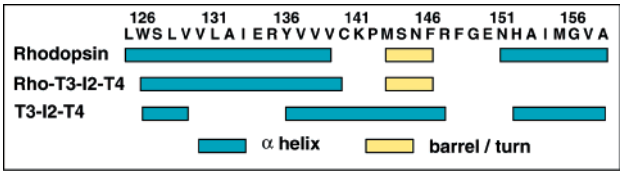

FIGURE 10: Comparison of secondary structure in rhodopsin and in the Rho-T3-I2-T4 peptide. The secondary structure over rhodopsin residues 125−158 is from the crystal structure (*1*). We based the secondary structure for the Rho-T3-I2-T4 peptide on the secondary shifts of the α protons and the pattern of NOEs. The α-helix locations of the T3-I2-T4 peptide are shown for comparison.

is to apply that structure and other experimental data to understand how GPCRs activate G proteins (*2*−*4*, *40*). Experimental structural data on the intracellular surface are thus timely and necessary to build accurate models of how GPCRs and G proteins interact, and to critically evaluate how well the GPCR prototype, rhodopsin, generalizes to other GPCRs.

An important consideration in this study is the meaningfulness of peptides as structural models. Since there is now a high-resolution structure of rhodopsin (*1*), a natural benchmark is to compare structures of rhodopsin peptides to that of the intact receptor. Our survey of the published secondary structures of rhodopsin intracellular loop peptides, determined by NMR (*41*−*43*), showed that the peptide termini are often disordered and lack helical structure present in the intact protein. In contrast, the middle regions of the peptides have stable secondary structure, β-turns, which resemble the structure in the rhodopsin loops. The disagreements likely arise because the peptide ends do not have enough constraints to maintain stable secondary structure. Therefore, we used longer peptides, with ends extending well into the TM helices. We also utilized micelle environments to interact with and stabilize the hydrophobic peptide termini. Piserchio et al. used this strategy to anchor the ends of a peptide from the parathyroid hormone receptor into a micelle and observed stable secondary structure at the peptide termini (*36*). With this approach, the Rho-T3-I2-T4 peptide demonstrated a stable helix similar to that of rhodopsin's TM3 helix (*1*) (Figure 10). The middle of the peptide (Met-143−Phe-146) contained NOEs that are consistent with a turn, in the same location as a turn referred to as a "barrel" in the crystal structure (*1*). Yeagle et al. also identified a β-turn in a similar position (Ser-144−Arg-147), in NMR studies on a shorter rhodopsin i2 peptide without the transmembrane anchors (*42*). Apparently, the 8 TM4 residues in Rho-T3-I2-T4 (as opposed to the 15 TM3 residues) are not sufficient to stabilize the TM4 helix in the peptide, since there was no helix at its C-terminus (Figure 10). Thus, the stable secondary structure that is actually in the Rho-T3-I2-T4 peptide is consistent with the secondary structure in rhodopsin. However, not all of the helix in rhodopsin is present in the peptide. Therefore, our peptide models are useful in determining, with high likelihood, a lower limit for helical structure in the intact protein.

From the above remarks, it is likely that the helices in the T3-I2-T4 peptide (Figure 9A) are present in the intact α2A AR. Helix α1 and helix α3 provide lower limit estimates of the cytoplasmic termini of the TM3 and TM4 helices, respectively, in the α2A AR. Since the WT and mutant T3-I2 peptides (Chung et al., manuscript submitted) and the T3-I2-T4 peptide (Chung et al., unpublished observations) are functionally active, potent stimulators of G protein activation, the three helices in T3-I2-T4 may represent the active i2 conformation in the α2A AR, which is believed to be less constrained (*44*).

The most important of our findings is that the peptide structures provide strong evidence that the majority of the α2A AR i2 loop contains a novel cytoplasmic helix, α2, not present in rhodopsin's i2 (*1*). Helix α2 is also not present in the Rho-T3-I2-T4 peptide and thus is unlikely to be a peptide artifact. This structural difference is significant, for it suggests that a major component of the α2A AR's binding surface for G proteins (*15*) differs from that of rhodopsin, and therefore their receptor−G protein interactions may be different. The result also implies that there is a need to reevaluate the use of rhodopsin structural data as a template for modeling the intracellular loops of other GPCRs, as has been done in the past (*9*, *11*).

Our results suggest but do not conclusively prove that when a cytoplasmic i2 helix is present there may be flexibility or a bend between it and the TM3 helix. If true, this means that the TM3 helix and the DRY motif within the i2 helix may not be aligned, which has relevance for models of GPCR activation that relate TM3 movements to the DRY motif. We cannot, however, predict how the flexibility or helical bend in the peptide will change in the context of the intact receptor.

The D130I mutation has subtle effects on the secondary structure surrounding the DRY motif in the T3-I2 peptide in micelles. The mutation also stabilizes the transmembrane helix α1, which may indicate a change in how the mutant peptide interacts with the micelles. Although we previously observed D130I mutation-induced structural changes in the T3-I2 peptide in lipid vesicles, by CD spectroscopy, the structural changes in micelles were too subtle to be detected by CD (Chung et al., submitted). These secondary structure changes may play a role in the ability of the D130I mutation to enhance the T3-I2 peptide's ability to stimulate G protein activation and, in the intact α2A adrenergic receptor, to increase agonist affinity 5-fold (Chung et al., submitted) without inducing the constitutive activity observed in other GPCRs (*12*, *14*, *45*). However, we cannot fully define the nature of such a role at present.

A remaining question is the extent to which this α2A AR structural model has relevance to other GPCRs. In this respect, a mutagenesis study on the m5 muscarinic receptor (mAchR) has also suggested that it has a helical i2 (*15*). That study showed that most of the residues in i2 are either functionally required for G protein activation or they cause constitutive activation upon mutation. When we mapped the two classes of residues onto the homologous residues in the structure of rhodopsin, they did not show any meaningful arrangement (Figure 7E,F). In contrast, when we mapped them onto the structure of the α2A AR T3-I2 determined in this report, they formed two clusters along the length of helix α2 (Figure 7C,D). Thus, it appears that the m5 mAchR and the α2A AR share the same structural motif in their i2, which is different than that of rhodopsin.

To look for a pattern to predict when a GPCR i2 loop will be helical, we aligned the i2 sequences of the α2A AR, the m5 mAchR, rhodopsin, and seven other randomly selected rhodopsin-like GPCRs (Table 1). We achieved no

Table 1: Compilation of Consensus Sequences, Functional and Structural Data, and Residue Polarity[e]

Sequence																														
Amino Acid Number		127	128	129	130	131	132	133	134	135	136	137	138	139	140	141	142	143	144	145	146	147	148	149	150	151	152	153
α2A AR	(Gi/Go/Gs)	I	S	L	D	R	Y	W	S	I	T	Q	A	I	E	Y	N	L	K	R	T	P	R	R	I	K	A	I
m5 mAchR	(Gq)	I	S	F	D	R	Y	F	S	I	T	R	P	L	T	Y	R	A	K	R	T	P	K	R	A	G	I	M
m2 mAchR	(Gi/Go)	I	S	F	D	R	Y	F	C	V	T	K	P	L	T	Y	P	V	K	R	T	T	K	M	A	G	M	M
5HT1A	(Gi/Go)	I	A	L	D	R	Y	W	A	I	T	D	P	I	D	Y	V	N	K	R	T	P	R	R	A	A	A	L
Rhodopsin	(Gt)	L	A	I	E	R	Y	V	V	V	C	K	P	M	S	N	F	R	F	G	E	N	H	-	A	I	M	G
β2 AR	(Gs)	I	A	V	D	R	Y	F	A	I	T	S	P	F	K	Y	Q	S	L	L	T	K	N	K	A	R	V	I
α1B AR	(Gq/Gi/Go)	I	S	I	D	R	Y	I	G	V	R	Y	S	L	Q	Y	P	T	L	V	T	R	R	K	A	I	L	A
H2	(Gs)	I	S	L	D	R	Y	C	A	V	T	D	P	L	R	Y	P	V	L	V	T	P	V	R	V	A	I	S
GRHR	(Gq)	I	S	L	D	R	S	L	A	I	T	R	P	L	A	L	K	S	N	S	K	V	G	Q	S	-	-	M
FPR	(Gi/Go)	I	A	L	D	R	C	V	C	V	L	H	P	V	W	T	Q	N	H	R	T	V	S	L	A	K	K	V
Conserved[a]		**I**	**S/A**		**D/E**	**R**	**Y**			**I/V**	T		P			**Y**					T						
Function[b]					♦	♦		θ		♦		θ	♦	♦	θ	θ	♦			θ	♦							
Residue Polarity[c]																												
Amino Acid No.		127	128	129	130	131	132	133	134	135	136	137	138	139	140	141	142	143	144	145	146	147	148	149	150	151	152	153
α2A AR	(Gi/Go/Gs)	N	P	N	P	P	I	I	P	N	P	P	N	N	P	I	P	N	P	P	P	N	P	P	N	P	N	N
m5 mAchR	(Gq)	N	P	N	P	P	I	N	P	N	P	P	N	N	P	I	P	N	P	P	P	N	P	P	N	N	N	I
m2 mAchR	(Gi/Go)	N	P	N	P	P	I	N	I	N	P	P	N	N	P	I	N	N	P	P	P	P	P	I	N	N	I	I
5HT1A	(Gi/Go)	N	N	N	P	P	I	I	N	N	P	P	N	N	P	I	N	P	P	P	P	N	P	P	N	N	N	N
Rhodopsin[d]	(Gt)	N	N	N	P	P	I	N	N	N	I	P	N	I	P	P	N	P	N	N	P	P	I	-	N	N	I	N
β2 AR[d]	(Gs)	N	N	N	P	P	I	N	N	N	P	P	N	P	P	I	P	P	N	N	P	P	P	P	N	P	N	N
α1B AR[d]	(Gq/Gi/Go)	N	P	N	P	P	I	N	N	N	P	I	P	N	P	I	N	P	N	N	P	P	P	P	N	N	N	N
H2[d]	(Gs)	N	P	N	P	P	I	I	N	N	P	P	N	N	P	I	N	N	N	N	P	N	N	P	N	N	N	P
GRHR	(Gq)	N	P	N	P	P	P	N	N	N	P	P	N	N	N	N	P	P	P	P	P	N	N	P	P	-	-	I
FPR	(Gi/Go)	N	N	N	P	P	I	N	I	N	N	I	N	N	I	P	P	P	I	P	P	N	P	N	N	P	P	N

[a] Boldface residues are conserved in rhodopsin-like GPCRs (*6*). Lightface residues are conserved in >60% of the GPCRs that we analyzed here. [b] Mutagenesis of the m5 mAchR (*15*) revealed functionally required residues (◆) and residues where mutations constitutively activate the receptor (*θ*). [c] Amino acids are grouped into highly polar (P) (hydroxyl, charged, amine groups), intermediate polarity (I) (aromatic and sulfur-containing), and nonpolar (N) (aliphatic) groups (*46*). Residues with the same polarity as the corresponding α2A AR residue are shaded. [d] These receptors are constitutively activated by mutations of the conserved Asp/Glu at position 130 (*12*−*14*, *45*). [e] Amino acid sequences of the i2 loop are listed for 10 rhodopsin-like GPCRs. The amino acid numbering is from the α2A AR. The receptors are as follows: α2A AR; m5 muscarinic (m5 mAchR); m2 muscarinic (m2 mAchR); 5HT1A serotonin (5HT1A); type I rhodopsin; *β*2 AR; α1B AR; histamine H2 (H2); gonadotropin-releasing hormone (GRHR); *N*-formyl peptide (FPR). The sequences are from humans, except for rhodopsin (bovine) and H2 (rat). The G protein specificity for each receptor is given in parentheses.

special insights based on residue conservation; however, when we classified i2 residues according to their polarity, following a method used by Lomize et al. to derive structural insights on GPCRs (*46*), striking patterns emerged (Table 1). There is 94% agreement in polarity between residues 133−149 of the α2A AR and the m5 mAchR, and only 29% agreement in polarity between the α2A AR and rhodopsin.

It is also evident from Table 1 that the nonpolar residues in the i2 of the α2A AR (spanning residues 133−149), the m2 and m5 mAchRs, and the serotonin receptor (5HT1AR) are spaced apart with helical periodicity. Therefore in the context of a helix, these nonpolar residues would satisfy the desire for residues of like polarity to cluster together in proteins (*46*), so as to avoid water exposure or to form a G protein-binding pocket. In contrast, rhodopsin, the α1B AR, the histamine H2 receptor, and, to a lesser degree, the *β*2 AR contain a unique pattern of nonpolar residues at positions 142, 144, and 145 (in the α2A AR numbering system, Table 1), which may cluster more readily in a loop structure, like that of rhodopsin's i2 (*1*). Thus, this simple identification of patterns in nonpolar i2 residues may be a predictor of structural propensities in the i2 loops of GPCRs. Furthermore, it is also interesting to note that the structural division correlates with a functional division. The four receptors mentioned that share rhodopsin's pattern of nonpolar residues are all constitutively activated by mutations at the conserved Asp/Glu, residue 130 (*12*−*14*, *45*). However, none of the α2A AR, the m5 mAchR, or the m1 mAchR, which also has the helical pattern of nonpolar i2 residues, is constitutively activated by Asp-130 mutations [Chung et al., submitted and (*15*, *47*)]. We speculate that the helical i2 in these receptors is the site of additional interactions that stabilize the inactive state of the receptors against constitutive activation.

In summary, the most important observation in this study was that the majority of the α2A AR second intracellular loop (i2) is a helix and that this helix is not present in the i2 of rhodopsin. This provides structural evidence that the intracellular loops of GPCRs, and hence the G protein-binding surface, contain structural differences with the

rhodopsin prototype. We also identified a simple method for predicting helical i2 loops in other GPCRs, based on patterns of nonpolar residues in i2. These experimental and theoretical observations will be of value in developing more accurate models of G protein coupled receptors and their interactions with G proteins.

ACKNOWLEDGMENT

We thank Professor Ayyalusamy Ramamoorthy of the University of Michigan Biophysics Research Division and Department of Chemistry for the generous use of his computer workstations and software for processing of the NMR data.

SUPPORTING INFORMATION AVAILABLE

A table containing resonance assignments is available free of charge via the Internet at http://pubs.acs.org.

REFERENCES

1. Palczewski, K., Kumasaka, T., Hori, T., Behnke, C. A., Motoshima, H., Fox, B. A., Trong, I. L., Teller, D. C., Okada, T., Stenkamp, R. E., Yamamoto, M., and Miyano, M. (2000) *Science 289*, 739−745.
2. Itoh, Y., Cai, K., and Khorana, H. G. (2001) *Proc. Natl. Acad. Sci. U.S.A. 98*, 4883−4887.
3. Cai, K., Itoh, Y., and Khorana, H. G. (2001) *Proc. Natl. Acad. Sci. U.S.A. 98*, 4877−4882.
4. Jang, G. F., Kuksa, V., Filipek, S., Bartl, F., Ritter, E., Gelb, M. H., Hofmann, K. P., and Palczewski, K. (2001) *J. Biol. Chem. 276*, 26148−26153.
5. Ballesteros, J. A., Shi, L., and Javitch, J. A. (2001) *Mol. Pharmacol. 60*, 1−19.
6. Baldwin, J. M., Schertler, G. F., and Unger, V. M. (1997) *J. Mol. Biol. 272*, 144−164.
7. Bourne, H. R., and Meng, E. C. (2000) *Science 289*, 733−734 (in Perspectives).
8. Probst, W. C., Snyder, L. A., Schuster, D. I., Brosius, J., and Sealfon, S. C. (1992) *DNA Cell Biol. 11*, 1−20.
9. Scheer, A., Fanelli, F., Costa, T., De Benedetti, P. G., and Cotecchia (1996) *EMBO J. 15*, 3566−3578.
10. Ballesteros, J., Kitanovic, S., Guarnieri, F., Davies, P., Fromme, B. J., Konvicka, K., Chi, L., Millar, R. P., Davidson, J. S., Weinstein, H., and Sealfon, S. C. (1998) *J. Biol. Chem. 273*, 10445−10453.
11. Fanelli, F. (2000) *J. Mol. Biol. 296*, 1333−1351.
12. Scheer, A., Fanelli, F., Costa, T., De Benedetti, P. G., and Cotecchia (1997) *Proc. Natl. Acad. Sci. U.S.A. 94*, 808−813.
13. Rasmussen, S. G., Jensen, A. D., Liapakis, G., Ghanouni, P., Javitch, J. A., and Gether, U. (1999) *Mol. Pharmacol. 56*, 175−184.
14. Acharya, S., and Karnik, S. S. (1996) *J. Biol. Chem. 271*, 25406−25411.
15. Burstein, E. S., Spalding, T. A., and Brann, M. R. (1998) *J. Biol. Chem. 273*, 24322−24327.
16. Eason, M. G., and Liggett, S. B. (1996) *J. Biol. Chem. 271*, 12826−12832.
17. Franke, R. R., Konig, B., Sakmar, T. P., Khorana, H. G., and Hofmann, K. P. (1990) *Science 250*, 123−125.
18. Dalman, H. M., and Neubig, R. R. (1991) *J. Biol. Chem. 266*, 11025−11029.
19. Munch, G., Dees, C., Hekman, M., and Palm, D. (1991) *Eur. J. Biochem. 198*, 357−364.
20. Konig, B., Arendt, A., McDowell, J. H., Kahlert, M., Hargrave, P. A., and Hofmann, K. P. (1989) *Proc. Natl. Acad. Sci. U.S.A. 86*, 6878−6882.
21. Fraser, C. M., Arakawa, S., McCombie, W. R., and Venter, J. C. (1989) *J. Biol. Chem. 264*, 11754−11761.
22. Wuthrich, K. (1986) *NMR of Proteins and Nucleic Acids*, John Wiley and Sons, New York.
23. Plateau, P., and Gueron, M. (1982) *J. Am. Chem. Soc. 104*, 7310−7311.
24. Piotto, M., Saudek, V., and Sklenar, V. (1992) *J. Biomol. NMR 2*, 661−665.
25. Marion, D., Ikura, M., Tshudin, R., and Bax, A. (1989) *J. Magn. Reson. 85*, 393−399.
26. Delaglio, F., Grzesiek, S., Vuister, G. W., Zhu, G., Pfeifer, J., and Bax, A. (1995) *J. Biomol. NMR 6*, 277−293.
27. Johnson, B. A., and Blevins, R. A. (1994) *J. Biomol. NMR 4*, 603−614.
28. Glaser, R. W., and Wuthrich, K. (2001) http://www.mol.biol.ethz.ch/wuthrich/software/spscan/.
29. Bartels, C., Xia, T., Billeter, M., Guntert, P., and Wuthrich, K. (1995) *J. Biomol. NMR 6*, 1−10.
30. Kim, Y., and Prestegard, J. H. (1989) *J. Magn. Reson. 84*, 9−13.
31. Guntert, P., Braun, W., and Wuthrich, K. (1991) *J. Mol. Biol. 217*, 517−530.
32. Guntert, P., Mumenthaler, C., and Wuthrich, K. (1997) *J. Mol. Biol. 273*, 283−298.
33. Guntert, P., Billeter, M., Wuthrich, K., and Brown, L. R. (1998) *J. Biomol. NMR 12*, 543−548.
34. Guntert, P., Berndt, K. D., and Wuthrich, K. (1993) *J. Biomol. NMR 3*, 601−606.
35. Henry, G. D., and Sykes, B. D. (1994) *Methods Enzymol. 239*, 515−535.
36. Piserchio, A., Bisello, A., Rosenblatt, M., Chorev, M., and Mierke, D. F. (2000) *Biochemistry 39*, 8153−8160.
37. Opella, S. J., Marassi, F. M., Gesell, J. J., Valente, A. P., Kim, Y., Oblatt-Montal, M., and Montal, M. (1999) *Nat. Struct. Biol. 6*, 374−379.
38. Wishart, D. S., Sykes, B. D., and Richards, F. M. (1992) *Biochemistry 31*, 1647−1651.
39. Cavanagh, J., Chazin, W. J., and Rance, M. (1990) *J. Magn. Reson. 87*, 110−131.
40. Hamm, H. E. (2001) *Proc. Natl. Acad. Sci. U.S.A. 98*, 4819−4821.
41. Yeagle, P. L., Alderfer, J. L., and Albert, A. D. (1995) *Biochemistry 34*, 14621−14625.
42. Yeagle, P. L., Alderfer, J. L., Salloum, A. C., Ali, L., and Albert, A. D. (1997) *Biochemistry 36*, 3864−3869.
43. Yeagle, P. L., Alderfer, J. L., and Albert, A. D. (1995) *Nat. Struct. Biol. 2*, 832−834.
44. Bourne, H. R. (1997) *Curr. Opin. Cell Biol. 9*, 134−142.
45. Alewijnse, A. E., Timmerman, H., Jacobs, E. H., Smit, M. J., Roovers, Cotecchia, S., and Leurs, R. (2000) *Mol. Pharmacol. 57*, 890−898.
46. Lomize, A. L., Pogozheva, I. D., and Mosberg, H. I. (1999) *J. Comput.-Aided Mol. Des. 13*, 325−353.
47. Lu, Z. L., Curtis, C. A., Jones, P. G., Pavia, J., and Hulme, E. C. (1997) *Mol. Pharmacol. 51*, 234−241.
48. Koradi, R., Billeter, M., and Wuthrich, K. (1996) *J. Mol. Graphics 14*, 51−55.

BI015811+